Enhancing the matrix-fiber interface with a surfactant leads to improved performance properties of 3D printed composite materials containing cellulose nanofibrils

Evan W. Battisto[1], Shea R. Sarsfield[1], Saurabh R. Lele[2], Teague Williams[3], Jeffrey M. Catchmark[1], Stephen C. Chmely[1]*

[1] Department of Agricultural and Biological Engineering, The Pennsylvania State University, University Park, PA 16802 USA

[2] Department of Food Science, The Pennsylvania State University, University Park, PA 16802 USA

[3] Materials Research Institute, The Pennsylvania State University, University Park, PA 16802 USA

KEYWORDS cellulose nanomaterial, surfactant, 3D printing, TOCNF, lauric arginate ethyl ester, stereolithography

ABSTRACT Cellulose nanofibrils (CNFs) exhibit characteristics that make them a desirable addition to new composite materials. CNFs are usable in a wide variety of applications such as coatings, personal and healthcare products, packaging, and advanced structural materials. They

can also help overcome some performance issues with objects 3D printed by stereolithography (SLA) including dimensional instability and poor mechanical properties. However, CNFs are hydrophilic, making their dispersion in hydrophobic resins common to SLA difficult. Therefore, improvement of performance properties will not be fully realized. In this work, we treated TEMPO-oxidized CNFs (TOCNFs) with the hydrochloride salt of lauroyl arginate ethyl ester (LAE·HCl), a cationic surfactant, to investigate how this coating would affect the performance properties of multicomponent uncured SLA resins and subsequently printed objects. We hypothesized this coating would enhance the dispersion of the cellulose nanomaterials when compared to their uncoated counterparts, which would lead to quantifiable differences among the sample groups. We found that the viscosity of a commercial 3D printing resin (0.34 Pa·s at 30 Hz) increased by nearly an order of magnitude upon addition of even 1 wt.%. uncoated TOCNFs (2.96 Pa·s at 30 Hz). Moreover, the tensile strength (19.9(5) MPa) and modulus (0.65(5) GPa) of objects printed from the commercial resin decreased when adding 4 wt.% uncoated TOCNF (12.5(2) MPa and 0.58(8) GPa, respectively). In contrast, resins having 4 wt.% TOCNFs coated with LAE were less viscous (1.25 Pa·s at 30 Hz), and objects printed from them had enhanced tensile strength (24.7(7) MPa) and modulus (0.78(8) GPa) when compared to both the unadulterated resin and that having uncoated TOCNFs. Our findings show the general utility of using a surfactant with cellulose nanomaterials to homogenize multicomponent resins for 3D printing composite materials with enhanced performance properties.

INTRODUCTION

Biorenewable products are those that can be created from renewable and living materials such as plants. These products have recently been the focus of intense research due to their potentially high value and enhanced performance with diminished environmental impact as compared to traditional petroleum-based products. Cellulose nanofibrils (CNFs) are a sustainable material used to develop bioproducts such as reinforced composites, high performance coatings, functional materials, and powder dispersions for several applications, including biorenewable plastics, food-grade products, healthcare, cosmetics, and more.[1–4] In contrast to cellulose nanocrystals (CNCs), CNFs typically have a high aspect ratio and contain both crystalline and amorphous domains.

Industrial application of CNFs can be enabled by methods to modify CNF surfaces, including mechanical, enzymatic, and chemical pretreatments.[5] TEMPO oxidation is one of the most common pretreatment methods, which oxidizes C6 to a carboxylic acid, making it available for further chemical modification. A well-known and widely studied process, TEMPO oxidation produces high-quality fibers with a moderate possibility of industrial implementation, given the quantity of chemical reagents used, the number of necessary processing steps, the cost of the pretreatment, and the energy required for nanofibrilation.[5]

TEMPO-oxidized cellulose nanofibril (TOCNF) films have exceptional mechanical properties, including Young's modulus of up to 14 GPa, tensile strength of up to 300 MPa, and strain to failure up to 10%.[6–11] Moreover, CNF-reinforced polymer composites of polyethylene oxide were 2.3 times stiffer and 1.9 times stronger than unadulterated PEO.[12] Long length and good matrix-fiber interactions were identified as reasons for this exceptional performance enhancement. Accordingly, TOCNFs have been widely investigated as the reinforcing fiber for several composite materials, including those created via 3D printing.[13]

3D printing is an umbrella term that encompasses several specific methods that build parts layer-by-layer. These vary based on materials used, surface morphology, resolution range, manufacturing speed, cost, and many others. Stereolithography (SLA) is a method that uses light to cure liquid resins into solid objects. The resins are mixtures of photocurable molecules that afford solid objects with smooth surfaces. However, SLA is limited by a narrow selection of resin materials, which are relatively hydrophobic.[14,15] This makes printing composite materials with hydrophilic cellulose nanofibrils especially challenging, given the interfacial mismatch between a hydrophilic fiber and a hydrophobic matrix.

Recent advances in photocured composites containing cellulose nanomaterials, including those generated via 3D printing by stereolithography, have been extensively reviewed.[16] Those incorporating nanofibrils include aerogels and/or hydrogels for tissue engineering,[17,18] cell adhesion,[19] and complex-shaped 3D printed scaffolds.[20] The major challenge identified in incorporating TOCNFs is the hydrophilic nature of nanocellulose and its affinity for aggregation via hydrogen bonding.[16] Accordingly, Sajab and coworkers showed that surface modification of CNF with PEO afforded enhanced mechanical properties to 3D printed composites. Polyurethane-based SLA resins modified with 3% CNF-PEO showed an increase in tensile strength (24%) and stiffness (10%), although weight loading above 3% CNF reduced the mechanical properties of the composites.[21]

Surfactants have also been used to enhance matrix-fiber interactions in nanocellulose-containing composites.[22–24] Surfactant molecules are amphiphilic, owing to the presence of both hydrophilic and hydrophobic functional groups, and charged[25,26] and non-ionic surfactants[27,28] have been used to lower the water wettability or enhance the dispersion of CNFs in polymer composites. In addition, members of our team have recently explored surface interactions between cationic

surfactant lauroyl arginate ethyl ester (LAE) and CNCs.[29] This surfactant is a food-grade antimicrobial derived from renewable materials,[30,31] and it exhibits excellent interactions with nanocellulose surfaces.

Despite the major challenge in incorporating TOCNFs into new photopolymer resins for 3D printing being a matrix-fiber mismatch, and despite the vast array of investigations regarding surfactant interactions with nanocellulose, no investigations to date have focused on using surfactants to enhance the nanointerfacial interactions between TOCNFs and 3D printer resins. Accordingly, here we present our findings related to using LAE to homogeneously disperse TOCNFs in a commercial 3D printer resin. We examine the surface hydrophobicity of coated TOCNFs, the rheological properties of 3D printer resins containing those TOCNFs, and the mechanical and morphological properties of objects printed using these new resins. Our findings indicate that employing a surfactant coating for TOCNFs enables 3D printing composite materials with enhanced performance properties when compared to both unadulterated resins and those containing unmodified TOCNFs.

MATERIALS AND METHODS

Reagents

Freeze-dried TEMPO-oxidized cellulose nanofibrils (TOCNFs, sodium form) were purchased from the University of Maine Process Development Center (Orono, ME USA). These TOCNFs were characterized by the manufacturer as having 1.49 mmol COONa per g dry TOCNF. CytoGuard LA 2X, a 20% (w/w) aqueous solution of the hydrochloride salt of lauric arginate ethyl ester (LAE), was kindly provided by A&B Ingredients, Inc. (Fairfield, NJ USA). SainSmart Rapid UV General Purpose Photopolymer Curing Resin (405 nm, transparent) was purchased from

Amazon.com, Inc. Ultrapure water (specific resistance, ϱ = 18.18 MΩ·cm) was used for all preparations. All reagents were used as received unless otherwise noted.

Preparation and characterization of LAE-coated TOCNFs

A 1% (w/w) dispersion of TOCNFs in water was produced by combining 3 g TOCNF (4.47 mmol COONa) with 297 g water. The resulting suspension was cooled to 0 °C (ice bath) and dispersed using an IKA T25 Digital ULTRA-TURRAX disperser (IKA Works, Inc., Wilmington, NC USA). The sample was dispersed at 15,000 rpm for 1 min and then allowed to rest for 1 min. This process was repeated 5 times. Then, the sample were sonicated at 0 °C (ice bath) using a VCX 750 laboratory scale ultrasonic processor (Sonics & Materials, Inc., Newtown, CT USA). The sample was pulsed at 20 kHz (80% amplitude) for five 30-s on/off cycles. The resulting homogeneous suspension was heated to 80 °C with stirring and 10.8 g Cytoguard LA 2X (5.14 mmol LAE·HCl, 15% mole excess vs COONa) was added by pouring over a period of 5 min to minimize foaming. The resulting mixture was allowed to stir overnight, after which it was frozen (-80 °C) and lyophilized using a Labconco FreeZone 2.5 benchtop freeze dry system (Labconco, Inc., Kansas City, MO USA) to afford a sticky off-white powder.

Coated and uncoated TOCNF samples were subjected to elemental analysis to measure the weight percent of total organic nitrogen (TON) using a Costech ECS 4010 CHNSO Analyzer (Costech Analytical Technologies, Inc., Valencia, CA USA). Coated samples were dialyzed (3.5 KDa) over a period of 4 days (water changed daily) to remove unbound surfactant. Diatomic nitrogen and carbon dioxide peak areas were measured using Isodat software and TON values were calculated using a peak area calibration based on a homogeneous caffeine standard. Error was determined by analyzing independent standards as samples across all EA runs.

Coated and uncoated TOCNF samples were also subjected to contact angle measurements to quantitatively measure surface wettability using a Ramé-Hart Model 295 Automated Goniometer/Tensiometer (Ramé-Hart Instrument Co., Succasunna, NJ USA). Solid TOCNFs were compressed into pellets (7.2 mm diameter × 0.55 mm thickness) and 5-uL water droplets were administered close to the surface of each pellet to prevent splashing and edge spinning. Contact angles of droplets were analyzed over 15 s with a secant method using Ramé-Hart's DropImg software.

Composite resin formulation and characterization

LAE-coated TOCNFs or uncoated TOCNFs were added to a known amount of SainSmart Rapid UV General Purpose Photopolymer Curing Resin to produce 40-g batches of composite resins having the weight percentages of 1, 2, 3, 4, 6, and 8% (w/w). The resulting resins were processed using the disperser and ultrasonic processor in a manner identical to that described above.

The rheological properties of the resins were measured using a TA Instruments HR-3 rheometer (TA Instruments, New Castle, DE USA) equipped with a double-wall geometry (inside bob diameter = 40.77 mm, outside bob diameter = 43.88 mm, inside cup diameter = 40.02 mm, outside cup diameter = 44.82 mm). Tests were performed over a range of shear rates from 0.1-30 Hz at 20 °C.

3D printing and mechanical testing

The resins were loaded into an Elegoo Mars Mono LCD MSLA Resin 3D Printer (Elegoo, Inc. Shenzhen, Guangdong China). The build platform was calibrated according to the manufacturer's instructions before each print, which consisted of 6 ASTM D638[32] Type-IV tensile testing specimens. Printing parameters were set up using CHITUBOX (CBD-Tech, Shenzhen,

Guangdong China) and were as follows: 12.5 μm layer height, 8 base layers, 30 s exposure time per base layer, 12 s exposure time per remaining layer.

Ultimate tensile strength and Young's modulus of the printed samples were measured using an Instron 5567 dual column universal testing machine. A 30-kN static load cell was used. Tests were performed following the ASTM D638 standard according to type IV specimen dimensions with a 1-mm/min extension rate for all tests. A one-way analysis of variance (ANOVA) was performed using Minitab to compare the effect of weight percentage of coated and uncoated TOCNFs on measured mechanical performance. Tukey's honest significant difference (HSD) test was performed using Minitab to reveal statistically significant differences among the samples.

RESULTS AND DISCUSSION

Surface modifications to prepared coated TOCNFs. We hypothesized that the guanidinium chloride head group in LAE would react with the sodium carboxylate groups decorating the surface of TOCNFs via a salt metathesis reaction to afford a surface coating of LAE as shown in Scheme 1 below. This hypothesis is supported by reports that indicate TOCNFs are neutralized by addition of even small amounts cationic surfactant based on ζ-potential measurements.[29,33–35] Accordingly, we treated TOCNFs having 1.49 mmol COONa per g dry TOCNF with a 15 mol% excess LAE·HCl to ensure complete transformation of all available sodium carboxylate sites to surface sites functionalized with LAE through hydrogen bonding interactions.

Scheme 1. Coating TOCNFs with LAE·HCl

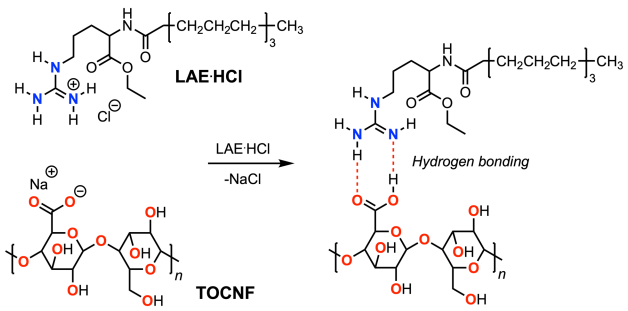

Since LAE contains 4 nitrogen atoms per molecule (Scheme 1), we investigated whether nitrogen elemental analysis would be a suitable technique to probe the amount of LAE coating each TOCNF. Given the presence of 1.49 mmol Na per g dry TOCNF, and 1 mmol LAE·HCl would theoretically interact with each mmol Na, it follows that 4 mmol of N would be present at each successfully substituted COONa site. As 1 mmol N atoms weighs 0.014007 g, 5.96 mmol N atoms (1.49 mmol × 4) weighs 0.0835 g; accordingly, a TOCNF with all 1.49 mmol COONa groups substituted with LAE would be approximately 8.35% (w/w) nitrogen. However, we measured the nitrogen content of the LAE-coated TOCNFs to be 3.23(7)%, suggesting that approximately 39% of the available COONa sites were substituted with LAE, despite adding a 15% (w/w) excess of LAE·HCl.

There are several possible factors that could influence this diminished substitution. First, we did not attempt to measure the accessibility of LAE·HCl to the COONa groups. Given the size of the tail portion of LAE (Scheme 1), and the flexibility of TOCNFs owing to their non-crystalline domains, it is reasonable to speculate that steric interactions could hinder the accessibility of the LAE·HCl to some portion of the available COONa sites.[24] Another factor could relate to the chemistry of the substitution. According to Le Chatelier's principle, a classical salt metathesis reaction is driven to completion by the formation of an insoluble salt and its subsequent precipitation from the reaction mixture. In the case of the reaction we describe, NaCl is formed in water, so there is potentially a greatly diminished thermodynamic driving force towards reaction completion because of the solubility of NaCl in water. Finally, qualitative analysis of the LAE-coated TOCNFs shows that the material is somewhat heterogeneous, meaning in the solid state, a non-uniform distribution of LAE on the TOCNFs could lead to isolation of a somewhat non-

representative sample for measurement by elemental analysis. Which of these (or other) factors (or their combination) that leads to a fractional LAE substitution is unclear.

Nevertheless, we were able to quantify a change in surface wettability between untreated TOCNFs and TOCNFs treated with LAE·HCl as described above (henceforth described as "coated" TOCNFs). As shown in Figure 1, contact angle measurements demonstrate a substantially increased surface hydrophobicity of coated TOCNFs as compared to the uncoated material. The mean contact angle of uncoated TOCNFs was measured to be 27.5(2)°, whereas that of the coated TOCNFs was measured to be 50(3)°, which corresponds to an approximately 82% increase in contact angle. This is an important result, as it suggests that LAE-coated TOCNFs would have enhanced dispersibility and matrix-fiber interfacial interactions in hydrophobic SLA resins. Together, these could lead to a measurable enhancement in performance properties of printed objects. We tested this hypothesis below.

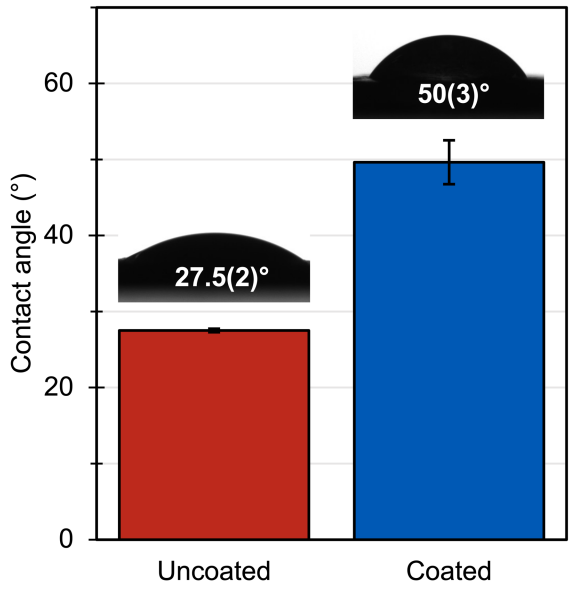

Figure 1. Contact angles of uncoated TOCNFs (red) and LAE-coated TOCNFs (blue). Values in parenthesis are standard error of the preceding digit. Images of the physical shapes of the water droplets at t = 15 s are provided.

Preparation of composite resins containing coated and uncoated TOCNFs. We dispersed the coated and uncoated TOCNFs in commercially available transparent 3D printer resin from SainSmart. For the coated TOCNFs, we blended composite resins containing 1, 2, 3, 4, 6, and 8% (w/w) TOCNFs. We also blended a composite resin containing 1% (w/w) uncoated TOCNFs to ascertain differences among the amounts of reinforcing nanomaterial and among coated and uncoated nanomaterials. Figure 2 summarizes the rheological properties of the resulting composite resins.

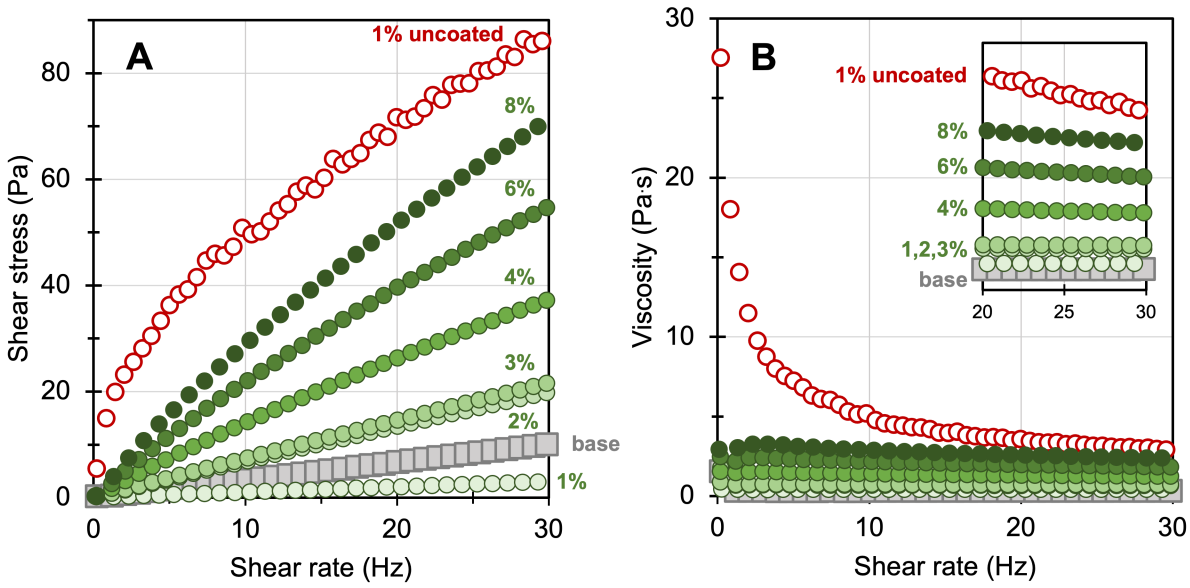

Figure 2. Flow curves (A) and viscosity curves (B) of the base commercial resin (gray squares), composite resins containing 1, 2, 3, 4, 6, and 8% (w/w) coated TOCNFs (filled green circles of increasing saturation), and a composite resin containing 1% (w/w) uncoated TOCNFs (unfilled red circles). The inset in panel B depicts the area between 20-30 Hz and 0-5 Pa·s.

As expected, the homogenous base resin (gray squares) displays ideal viscous flow behavior. In this case, viscosity is independent of shear rate (as is evident by the linear plot of shear stress vs shear rate in the flow curve shown in Figure 2A) because the commercial resin is a homogenous mixture of relatively low molecular weight materials. Moreover, resins containing 1-3% (w/w) coated TOCNFs display similar ideal viscous flow behavior (Figure 2A), albethey with nominally higher viscosities when compared to the base resin (Figure 2B inset and Table 1 below).

For composite resins containing 4, 6, and 8% (w/w) coated TOCNFs, the flow behavior of the resulting pseudoplastic fluids deviates slightly from ideal viscous flow by displaying shear thinning behavior (Figure 2A). This is evident from the viscosity curves for those materials, which display a decrease in viscosity with as shear rate increases (Figure 2B inset). This perhaps suggests that as we add additional coated TOCNFs, the homogeneity of the resulting dispersion decreases somewhat.

The most convincing evidence for the homogeneous dispersion of TOCNFs imparted by coating them with LAE comes from comparing the flow curves of the 1% (w/w) coated and uncoated composite resins. Even at low uncoated TOCNF concentration, the composite resin displays shear thinning behavior (Figure 2A, unfilled red circles), and the viscosity at very low shear rates (below 1 Hz) is outside the specified range of allowable viscosities for most commercially available 3D printers.[14] This is in stark contrast to the composite resin containing 1% (w/w) coated TOCNFs, which is evidently relatively homogeneous when compared to the composite resin containing uncoated TOCNFs. In fact, even the composite resin containing 8% (w/w) coated TOCNFs (the maximum loading we studied here) has an apparent viscosity at a shear rate of 30 Hz below that of the composite resin containing 1% (w/w) uncoated TOCNFs, despite containing nearly an order of magnitude more TOCNFs.

Ultimately, the rheological properties of SLA resins are important to their success in 3D printing solid objects. During 3D printing by SLA, the build platform to which the forming part is adhered slowly moves up and down through the liquid resin bath. As a result, growing parts are constantly coated and uncoated with uncured liquid resin. Accordingly, the operating viscosities and shear rates for stereolithography are relatively low (30-100 Hz depending on the printer manufacturer and printing parameters).[36] This ensures maximal part resolution by retaining a minimal amount of uncured resin between layer curing, as low-viscosity resin easily runs off parts during printing. This is perhaps analogous to applying multiple thin coats of paint to a wall rather than one thick, uneven coat. Accordingly, we report the measured apparent viscosities at 30 Hz of all the resins in Table 1 below and note the tested composite resins fall below the 5 Pa·s limit commonly associated with SLA printers.

Table 1. Apparent viscosities of composite SLA resins measured at 30 Hz

Resin	Apparent Viscosity @ 30 Hz (Pa·s)
0	0.34
1% coated	0.34
2% coated	0.64
3% coated	0.72
4% coated	1.25
6% coated	1.83
8% coated	2.37
1% uncoated	2.90

Investigation of mechanical properties and morphology of 3D printed parts. We 3D printed tensile testing specimens according to the ASTM D638 standard using a commercially available

desktop 3D printer and measured Young's modulus (stiffness) and ultimate tensile strength of the printed materials using static tensile testing. We then performed a one-way analysis of variance (ANOVA) with a subsequent Tukey's test of honestly significant differences (HSD) to determine statistical differences among the measured performance properties of the various testing specimens. The results of these tests are summarized in Figure 3.

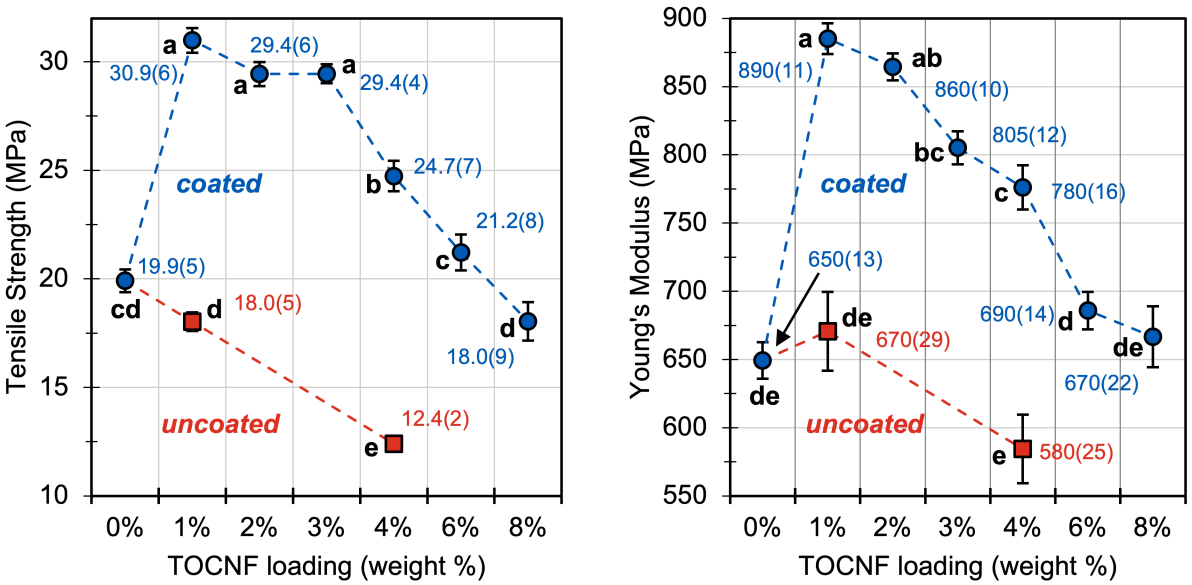

Figure 3. Plots of tensile strength (left) and Young's modulus (right) of 3D printed tensile testing specimens containing various weight percentages of coated (blue circles) and uncoated (red squares) TOCNFs. Each measurement was performed 6 times on 3 different mixtures as displayed for a total of 18 measurements per data point. The means (markers and values) and standard error of the means (error bars and parenthetical values) are shown. Tukey's test of honestly significant differences (HSD) was used to determine statistical differences among the samples (letters a-e); samples that are not statistically different share letters. The dotted lines are not mathematically meaningful and are provided only to guide the eye.

As shown in Figure 3, small amounts of uncoated TOCNFs (1% (w/w), red markers) do not have a statistically significant effect on the tensile strength or the stiffness of the printed composites. A higher 4% (w/w) loading of uncoated TOCNFs is detrimental to the material properties of printed objects, which shows a decrease in tensile strength and stiffness of 38 and 11%, respectively. We attribute these results to the heterogeneous nature of the pre-printed liquid resins, which are evidenced by their pseudoplastic rheological behavior (see above). In fact, we were unable to measure the viscosity of the composite resin containing 4% (w/w) uncoated TOCNFs, and it was visibly heterogenous after blending.

In contrast to the composites that contain uncoated TOCNFs, those that contain coated TOCNFs display marked improvement in tensile strength and stiffness. The greatest improvement in mechanical properties came at the lowest loadings of coated TOCNFs (1, 2, and 3% (w/w)). This result aligns with the rheological behavior of those ideally viscous liquid resins (see above). As we add additional coated TOCNFs (4, 6, and 8% (w/w)), the mechanical properties begin to degrade. Again, this parallels the rheological results, which indicate a pseudoplastic behavior of the liquid resins caused by resin heterogeneity.

In addition to tensile testing specimens, we also printed a so-called "torture test" print that was provided by user KCSteve on thingiverse.com.[37] Torture tests incorporate print features that are challenging to resolve with a given resin combination. In our case, we were interested in discerning how resin viscosity affects negative features (holes) in prints. All other parameters being equal (e.g. exposure time, light-off delay, build platform velocity, etc.), any differences in print morphology can be attributed to differences in the resins used. Photographs of these prints using resin containing 1% (w/w) coated and uncoated TOCNFs are provided in Figure 4.

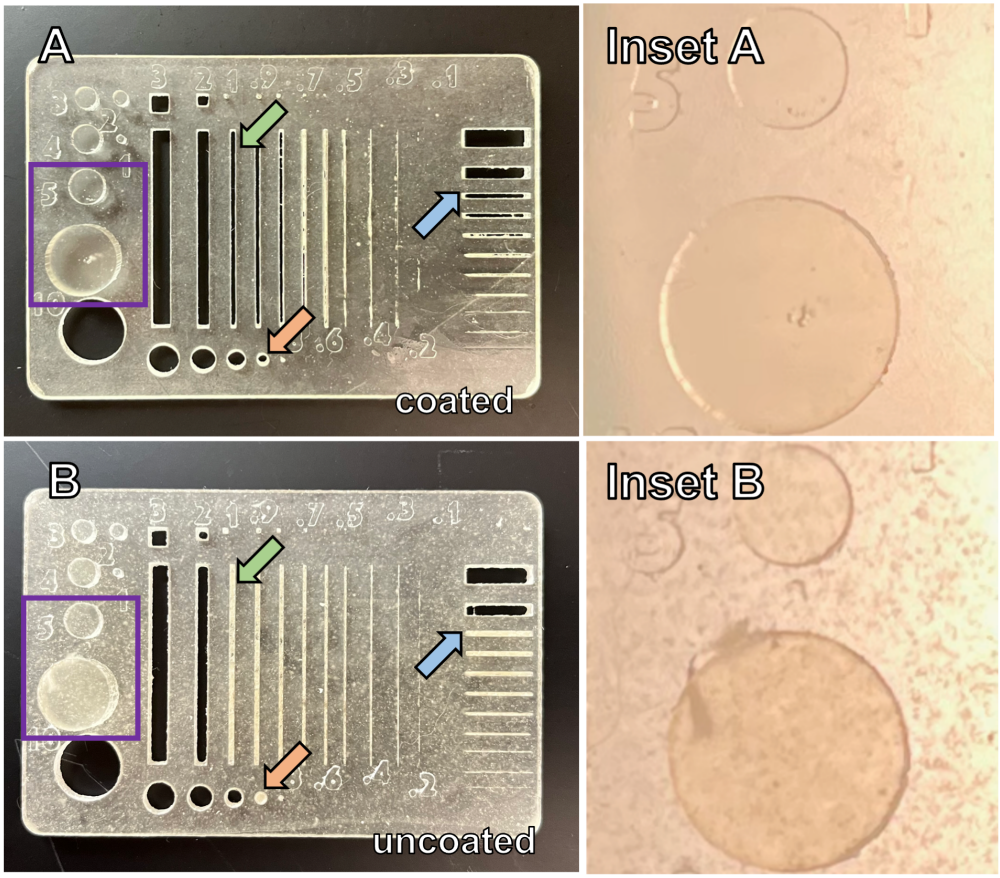

Figure 4. Torture test specimens containing 1% (w/w) coated (A) and uncoated (B) TOCNFs. The purple square (insets) and green, orange, and blue arrows are points of comparison that highlight the resin performance differences.

As shown in Figure 4, the surface finish of the prints is markedly different when using the resin containing coated or uncoated TOCNFs. The resin containing coated TOCNFs is much smoother, and the part appears clearer and more homogenous (Figure 4A, purple square inset). In contrast, the resin containing uncoated TOCNFs has a rough surface finish, and the part is cloudy, likely due to agglomeration of the TOCNFs (Figure 4B, purple square inset). In addition, we noted distinct differences in our ability to resolve small negative features in the *xy* plane (parallel to the build platform) of printed parts. We could resolve smaller holes in the vertical (green arrows) and horizontal (blue arrows) directions, and we could resolve smaller circular holes (orange arrows)

using the resin containing coated TOCNFs. We attribute this to the ability of the resin to drain from these features during printing because of its lower viscosity (see above).

Matrix-fiber interaction discussion. In the case of resins containing *uncoated* TOCNFs, inter- and intra-fiber interactions via hydrogen bonding are more prevalent than interactions between the photopolymer matrix and the dispersed TOCNF reinforcing fiber. Although the commercial resin we used has a proprietary composition that is unknown to us, it is likely composed of a mixture acrylate monomers and oligomers. Acrylate monomers are overwhelmingly used in commercial 3D printing resins because of their favorable polymerization kinetics and low cost.[14] Therefore, the interfacial mismatch between the relatively hydrophilic surface of the TOCNF fibers and the relatively hydrophobic surface of the cured polyacrylate photopolymer affords minimal stress transfer between the matrix and the fiber, leading to no change in mechanical properties of composites with low amounts of uncoated TOCNFs (1% (w/w)). At higher loadings of uncoated fibers (4% (w/w)), substantial agglomeration could form what are essentially discontinuities in the polyacrylate matrix due to a lack of wettability and mixing, which leads to severe degradation of performance properties.

In contrast, for the case of lower loadings of *coated* materials, the relatively homogenous resins contain well dispersed TOCNFs, which lead to a substantial boost to performance properties. This improvement occurs via an enhancement of matrix-fiber interactions between the cured photopolymer matrix and the dispersed TOCNF reinforcing fiber. This is due to the presence of the surfactant on the surface of the TOCNFs, which homogenizes the interfacial layer by interacting with the hydrophilic TOCNF surface via hydrogen bonding (Scheme 1) and the hydrophobic polyacrylate matrix via non-covalent dispersion interactions. As we increase the amount of coated TOCNFs, the resulting pseudoplastic resins are less homogeneous because inter-

and intra-fiber hydrogen bonding interactions begin to dominate. This is perhaps due to an incomplete substitution of surface COONa groups via our salt metathesis method (see above). We therefore recognize an opportunity to optimize the surface coating step using LAE or other surfactants, which could further improve fiber dispersion and resulting performance properties. We are currently investigating these phenomena further in our lab.

CONCLUSIONS

In this work, we investigated nanocellulose-containing composite materials that were 3D printed via stereolithography. We demonstrated that LAE, a widely used and commercially available surfactant, could be used to coat the surface of TEMPO-oxidized cellulose nanofibrils. The presence of this coating led to a substantial improvement in performance properties of 3D printed composites, likely due to enhancement of interfacial interactions between the matrix and fiber phases. Moreover, the coating also provided enhanced resolution to printed parts, especially related to negative features, when compared to resins containing TOCNFs without the coating. Overall, this strategy is generally applicable to dispersion of hydrophilic cellulose nanomaterials in common hydrophobic SLA resins and could lead to high performance renewable biocomposites via additive manufacturing. Our future work will focus on using this strategy to 3D print new composite materials with additional bioderived polymers such as lignin.

AUTHOR INFORMATION

Corresponding Author

*Email: sc411@psu.edu. Tel: +1 (814) 863-6815

Author Contributions

The manuscript was written through contributions of all authors. All authors have given approval to the final version of the manuscript.

Notes

The authors declare no competing financial interest.

ACKNOWLEDGMENT

This project was supported by funds provided by the Southeastern Sun Grant Center and the US Department of Transportation, Research and Innovative Technology Administration DTOS59-07-00050. SCC and JMC acknowledge support from the USDA National Institute of Food and Agriculture Federal Appropriations under Project PEN04671 and Accession number 1017582.

REFERENCES

(1) Dufresne, A. Nanocellulose: A New Ageless Bionanomaterial. *Mater. Today* **2013**, *16* (6), 220–227. https://doi.org/10.1016/j.mattod.2013.06.004.

(2) Nechyporchuk, O.; Belgacem, M. N.; Bras, J. Production of Cellulose Nanofibrils: A Review of Recent Advances. *Ind. Crops Prod.* **2016**, *93*, 2–25. https://doi.org/10.1016/j.indcrop.2016.02.016.

(3) Lavoine, N.; Desloges, I.; Dufresne, A.; Bras, J. Microfibrillated Cellulose – Its Barrier Properties and Applications in Cellulosic Materials: A Review. *Carbohydr. Polym.* **2012**, *90* (2), 735–764. https://doi.org/10.1016/j.carbpol.2012.05.026.

(4) Klemm, D.; Kramer, F.; Moritz, S.; Lindström, T.; Ankerfors, M.; Gray, D.; Dorris, A. Nanocelluloses: A New Family of Nature-Based Materials. *Angew. Chem. Int. Ed.* **2011**, *50* (24), 5438–5466. https://doi.org/10.1002/anie.201001273.

(5) Rol, F.; Belgacem, M. N.; Gandini, A.; Bras, J. Recent Advances in Surface-Modified Cellulose Nanofibrils. *Prog. Polym. Sci.* **2019**, *88*, 241–264. https://doi.org/10.1016/j.progpolymsci.2018.09.002.

(6) Saito, T.; Hirota, M.; Tamura, N.; Kimura, S.; Fukuzumi, H.; Heux, L.; Isogai, A. Individualization of Nano-Sized Plant Cellulose Fibrils by Direct Surface Carboxylation Using TEMPO Catalyst under Neutral Conditions. *Biomacromolecules* **2009**, *10* (7), 1992–1996. https://doi.org/10.1021/bm900414t.

(7) Isogai, A.; Saito, T.; Fukuzumi, H. TEMPO-Oxidized Cellulose Nanofibers. *Nanoscale* **2011**, *3* (1), 71–85. https://doi.org/10.1039/C0NR00583E.

(8) Fujisawa, S.; Okita, Y.; Fukuzumi, H.; Saito, T.; Isogai, A. Preparation and Characterization of TEMPO-Oxidized Cellulose Nanofibril Films with Free Carboxyl Groups. *Carbohydr. Polym.* **2011**, *84* (1), 579–583. https://doi.org/10.1016/j.carbpol.2010.12.029.

(9) Moon, R. J.; Martini, A.; Nairn, J.; Simonsen, J.; Youngblood, J. Cellulose Nanomaterials Review: Structure, Properties and Nanocomposites. *Chem. Soc. Rev.* **2011**, *40* (7), 3941–3994. https://doi.org/10.1039/C0CS00108B.

(10) Benítez, A. J.; Torres-Rendon, J.; Poutanen, M.; Walther, A. Humidity and Multiscale Structure Govern Mechanical Properties and Deformation Modes in Films of Native Cellulose Nanofibrils. *Biomacromolecules* **2013**, *14* (12), 4497–4506. https://doi.org/10.1021/bm401451m.

(11) Forti, E. S.; Moon, R. J.; Schueneman, G. T.; Youngblood, J. P. Transparent Tempo Oxidized Cellulose Nanofibril (TOCNF) Composites with Increased Toughness and Thickness by Lamination. *Cellulose* **2020**, *27* (8), 4389–4405. https://doi.org/10.1007/s10570-020-03107-8.

(12) Xu, X.; Liu, F.; Jiang, L.; Zhu, J. Y.; Haagenson, D.; Wiesenborn, D. P. Cellulose Nanocrystals vs. Cellulose Nanofibrils: A Comparative Study on Their Microstructures and Effects as Polymer Reinforcing Agents. *ACS Appl. Mater. Interfaces* **2013**, *5* (8), 2999–3009. https://doi.org/10.1021/am302624t.

(13) Ee, L. Y.; Li, S. F. Y. Recent Advances in 3D Printing of Nanocellulose: Structure, Preparation, and Application Prospects. *Nanoscale Adv.* **2021**, *3* (5), 1167–1208. https://doi.org/10.1039/D0NA00408A.

(14) Black, Hayden Thompson; Celina, Mathias C.; McElhanon, James R. *Additive Manufacturing of Polymers: Materials Opportunities and Emerging Applications*; SAND2016-6644; Sandia National Laboratories: Albuquerque, NM, 2016.

(15) Melchels, F. P. W.; Feijen, J.; Grijpma, D. W. A Review on Stereolithography and Its Applications in Biomedical Engineering. *Biomaterials* **2010**, *31* (24), 6121–6130. https://doi.org/10.1016/j.biomaterials.2010.04.050.
(16) Poothanari, M. A.; Schreier, A.; Missoum, K.; Bras, J.; Leterrier, Y. Photocured Nanocellulose Composites: Recent Advances. *ACS Sustain. Chem. Eng.* **2022**, *10* (10), 3131–3149. https://doi.org/10.1021/acssuschemeng.1c07631.
(17) Sun, D.; Liu, W.; Tang, A.; Guo, F.; Xie, W. A New PEGDA/CNF Aerogel-Wet Hydrogel Scaffold Fabricated by a Two-Step Method. *Soft Matter* **2019**, *15* (40), 8092–8101. https://doi.org/10.1039/C9SM00899C.
(18) Tang, A.; Ji, J.; Li, J.; Liu, W.; Wang, J.; Sun, Q.; Li, Q. Nanocellulose/PEGDA Aerogels with Tunable Poisson's Ratio Fabricated by Stereolithography for Mouse Bone Marrow Mesenchymal Stem Cell Culture. *Nanomaterials* **2021**, *11* (3), 603. https://doi.org/10.3390/nano11030603.
(19) Sun, X.; Tyagi, P.; Agate, S.; McCord, M. G.; Lucia, L. A.; Pal, L. Highly Tunable Bioadhesion and Optics of 3D Printable PNIPAm/Cellulose Nanofibrils Hydrogels. *Carbohydr. Polym.* **2020**, *234*, 115898. https://doi.org/10.1016/j.carbpol.2020.115898.
(20) Hausmann, M. K.; Siqueira, G.; Libanori, R.; Kokkinis, D.; Neels, A.; Zimmermann, T.; Studart, A. R. Complex-Shaped Cellulose Composites Made by Wet Densification of 3D Printed Scaffolds. *Adv. Funct. Mater.* **2020**, *30* (4), 1904127. https://doi.org/10.1002/adfm.201904127.
(21) Mohan, D.; Sajab, M. S.; Kaco, H.; Bakarudin, S. B.; Mohamed Noor, A. 3D Printing of UV-Curable Polyurethane Incorporated with Surface-Grafted Nanocellulose. *Nanomaterials* **2019**, *9* (12), 1726. https://doi.org/10.3390/nano9121726.
(22) Shamsuri, A. A.; Md. Jamil, S. N. A. Functional Properties of Biopolymer-Based Films Modified with Surfactants: A Brief Review. *Processes* **2020**, *8* (9), 1039. https://doi.org/10.3390/pr8091039.
(23) Hubbe, M. A.; Rojas, O. J.; Lucia, L. A. Green Modification of Surface Characteristics of Cellulosic Materials at the Molecular or Nano Scale: A Review. *BioResources* **2015**, *10* (3), 6095–6206.
(24) Tardy, B. L.; Yokota, S.; Ago, M.; Xiang, W.; Kondo, T.; Bordes, R.; Rojas, O. J. Nanocellulose–Surfactant Interactions. *Curr. Opin. Colloid Interface Sci.* **2017**, *29*, 57–67. https://doi.org/10.1016/j.cocis.2017.02.004.
(25) Mattina, M. J. I.; Berger, W. A. I.; Denson, C. L. Microwave-Assisted Extraction of Taxanes from Taxus Biomass. *J. Agric. Food Chem.* **1997**, *45* (12), 4691–4696. https://doi.org/10.1021/jf970454o.
(26) Syverud, K.; Xhanari, K.; Chinga-Carrasco, G.; Yu, Y.; Stenius, P. Films Made of Cellulose Nanofibrils: Surface Modification by Adsorption of a Cationic Surfactant and Characterization by Computer-Assisted Electron Microscopy. *J. Nanoparticle Res.* **2011**, *13* (2), 773–782. https://doi.org/10.1007/s11051-010-0077-1.
(27) Zimmermann, M. V. G.; da Silva, M. P.; Zattera, A. J.; Campomanes Santana, R. M. Effect of Nanocellulose Fibers and Acetylated Nanocellulose Fibers on Properties of Poly(Ethylene-Co-Vinyl Acetate) Foams. *J. Appl. Polym. Sci.* **2017**, *134* (17). https://doi.org/10.1002/app.44760.
(28) Bauli, C. R.; Rocha, D. B.; Rosa, D. dos S. Composite Films of Ecofriendly Lignocellulosic Nanostructures in Biodegradable Polymeric Matrix. *SN Appl. Sci.* **2019**, *1* (7), 774. https://doi.org/10.1007/s42452-019-0765-0.

(29) Chi, K.; Catchmark, J. M. Crystalline Nanocellulose/Lauric Arginate Complexes. *Carbohydr. Polym.* **2017**, *175*, 320–329. https://doi.org/10.1016/j.carbpol.2017.08.005.
(30) Asker, D.; Weiss, J.; McClements, D. J. Analysis of the Interactions of a Cationic Surfactant (Lauric Arginate) with an Anionic Biopolymer (Pectin): Isothermal Titration Calorimetry, Light Scattering, and Microelectrophoresis. *Langmuir* **2009**, *25* (1), 116–122. https://doi.org/10.1021/la803038w.
(31) Pinazo, A.; Manresa, M. A.; Marques, A. M.; Bustelo, M.; Espuny, M. J.; Pérez, L. Amino Acid–Based Surfactants: New Antimicrobial Agents. *Adv. Colloid Interface Sci.* **2016**, *228*, 17–39. https://doi.org/10.1016/j.cis.2015.11.007.
(32) *Standard Test Method for Tensile Properties of Plastics*. https://www.astm.org/d0638-14.html (accessed 2022-06-29).
(33) Hossain, K. M. Z.; Calabrese, V.; da Silva, M. A.; Bryant, S. J.; Schmitt, J.; Scott, J. L.; Edler, K. J. Cationic Surfactants as a Non-Covalent Linker for Oxidised Cellulose Nanofibrils and Starch-Based Hydrogels. *Carbohydr. Polym.* **2020**, *233*, 115816. https://doi.org/10.1016/j.carbpol.2019.115816.
(34) Quennouz, N.; Hashmi, S. M.; Choi, H. S.; Kim, J. W.; Osuji, C. O. Rheology of Cellulose Nanofibrils in the Presence of Surfactants. *Soft Matter* **2015**, *12* (1), 157–164. https://doi.org/10.1039/C5SM01803J.
(35) Prathapan, R.; Thapa, R.; Garnier, G.; Tabor, R. F. Modulating the Zeta Potential of Cellulose Nanocrystals Using Salts and Surfactants. *Colloids Surf. Physicochem. Eng. Asp.* **2016**, *509*, 11–18. https://doi.org/10.1016/j.colsurfa.2016.08.075.
(36) Elbadawi, M. *Polymeric Additive Manufacturing: The Necessity and Utility of Rheology*; IntechOpen, 2018. https://doi.org/10.5772/intechopen.77074.
(37) Thingiverse.com. *Printer Resolution Test Plates by KCSteve*. https://www.thingiverse.com/thing:420781 (accessed 2022-06-29).

For Table of Contents Only